

Electromagnetic probes of dense matter in heavy-ion collisions*

G.Q. Li^a, G.E. Brown^a, and C.M. Ko^b

^aDepartment of Physics, State University of New York at Stony Brook,
Stony Brook, NY 11793, USA

^bCyclotron Institute and Physics Department, Texas A&M University,
College Station, TX 77843, USA

Dilepton and photon production in heavy-ion collisions at SPS energies are studied in the relativistic transport model that incorporates self-consistently the change of hadron masses in dense matter. It is found that the dilepton spectra in proton-nucleus reactions can be well described by the conventional mechanism of Dalitz decay and direct vector meson decay. However, to provide a quantitative explanation of the observed dilepton spectra in central heavy-ion collisions requires contributions other than these direct decays and also various medium effects. Introducing a decrease of vector meson masses in hot dense medium, we find that these heavy-ion data can be satisfactorily explained. Furthermore, the single photon spectra in our calculations with either free or in-medium meson masses do not exceed the upper bound deduced from the experiments by the WA80 Collaboration.

1. INTRODUCTION

The measurement of electromagnetic observables such as the photon and dilepton spectra constitutes a major part of CERN-SPS heavy-ion programs. It will soon become one of major efforts at the BNL-RHIC heavy-ion programs. The primary reason for this is that photons and dileptons do not suffer strong final-state interactions as hadrons do. They can thus be considered as ‘penetrating probes’ of the initial hot and dense stages involved in high-energy heavy-ion collisions.

Recent observation of the enhancement of low-mass dileptons in central heavy-ion collisions at CERN-SPS energies [1,2] has generated a great deal of interest in the heavy-ion community. Different dynamical models, such as the hydrodynamical and transport models, have been used to investigate this phenomenon [3–12]. Calculations based on ‘conventional sources’ such as the Dalitz decay and direct vector meson decay that account for the dilepton spectra in proton-induced reactions failed to explain the observed enhancement in heavy-ion collisions. Various medium effects, such as the dropping vector meson masses [3,4,9,11] as first proposed by Brown and Rho [13], the modification of rho meson spectral function [6], and the enhanced production of η and/or η' [14], have

*Work supported by the Department of Energy under grant No. DE-FG-88ER40388 and by the National Science Foundation under grant No. PHY-9509266

been proposed to explain this enhancement. The last possibility has been ruled out by the measured η spectra in the same reactions [15]. The effects due to medium modifications of rho meson spectral function on low-mass dileptons have been examined using simplified fireball models [6]; questions remain concerning the exact space-time evolution and baryon chemical compositions which play an important role in the determination of the rho meson spectral function. In this contribution we will concentrate on the idea of dropping vector meson masses, which is the focus of Section 3.

Another piece of experimental data from CERN-SPS that has been discussed extensively is the single photon spectra from the WA80 collaboration [16]. In various hydrodynamics calculations the absence of significant thermal photon production has been used as an indication of quark gluon plasma formation that lowers the initial temperature [17]. However, detailed transport model calculations find this conclusion to be premature. This will be discussed in Section 4. A brief summary is given in Section 5.

2. THE RELATIVISTIC TRANSPORT MODEL

In studying medium effects in heavy-ion collisions, the relativistic transport model [18] based on the Walecka-type model [19] has been quite useful, as it provides a thermodynamically consistent description of the medium effects through the scalar and vector fields. In heavy-ion collisions at CERN-SPS energies, many hadrons are produced in the initial nucleon-nucleon interactions. This is usually modeled by the fragmentation of strings, which are the chromoelectric flux-tubes excited from the interacting quarks. One successful model for taking into account this nonequilibrium dynamics is the RQMD model [20]. To extend the relativistic transport model to heavy-ion collisions at these energies, we have used as initial conditions the hadron abundance and distributions obtained from the string fragmentation in RQMD. Further interactions and decays of these hadrons are then taken into account as in usual relativistic transport model.

To study the effects of dropping vector meson masses [13,21] on the dilepton spectrum in heavy-ion collisions, we have extended the Walecka model from the coupling of nucleons to scalar and vector fields to the coupling of light quarks to these fields, using the ideas of the meson-quark coupling model [22]. For a system of nucleons, pseudoscalar mesons, vector mesons, and axial-vector mesons at temperature T and baryon density ρ_B , the scalar field $\langle\sigma\rangle$ is determined self-consistently from

$$\begin{aligned}
m_\sigma^2\langle\sigma\rangle &= \frac{4g_\sigma}{(2\pi)^3} \int d\mathbf{k} \frac{m_N^*}{E_N^*} \left[\frac{1}{\exp((E_N^* - \mu_B)/T) + 1} + \frac{1}{\exp((E_N^* + \mu_B)/T) + 1} \right] \\
&+ \frac{0.45g_\sigma}{(2\pi)^3} \int d\mathbf{k} \frac{m_\eta^*}{E_\eta^*} \frac{1}{\exp(E_\eta^*/T) - 1} + \frac{6g_\sigma}{(2\pi)^3} \int d\mathbf{k} \frac{m_\rho^*}{E_\rho^*} \frac{1}{\exp(E_\rho^*/T) - 1} \\
&+ \frac{2g_\sigma}{(2\pi)^3} \int d\mathbf{k} \frac{m_\omega^*}{E_\omega^*} \frac{1}{\exp(E_\omega^*/T) - 1} + \frac{6\sqrt{2}g_\sigma}{(2\pi)^3} \int d\mathbf{k} \frac{m_{a_1}^*}{E_{a_1}^*} \frac{1}{\exp(E_{a_1}^*/T) - 1}, \quad (1)
\end{aligned}$$

where we have used the constituent quark model relations for the nucleon and vector meson masses [22], i.e., $m_N^* = m_N - g_\sigma\langle\sigma\rangle$, $m_{\rho,\omega}^* \approx m_{\rho,\omega} - (2/3)g_\sigma\langle\sigma\rangle$, the quark structure of the η meson in free space which leads to $m_\eta^* \approx m_\eta - 0.45g_\sigma\langle\sigma\rangle$, and the Weinberg sum rule relation between the rho-meson and a_1 meson masses, i.e., $m_{a_1}^* \approx m_{a_1} - (2\sqrt{2}/3)g_\sigma\langle\sigma\rangle$.

We recently found that the use of a refined model, the effective chiral Lagrangian of [23], led to essentially the same results for dilepton spectra [24].

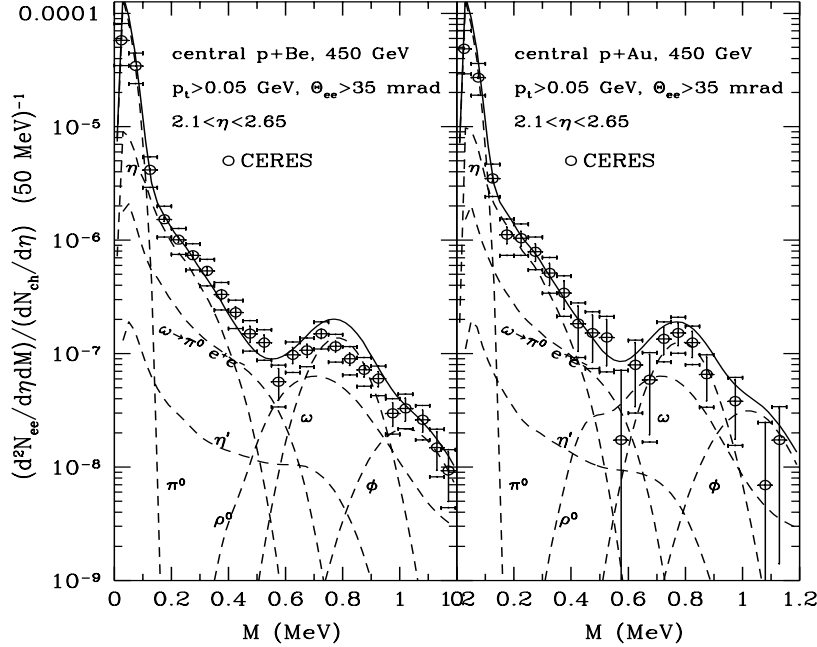


Figure 1. Dilepton invariant mass spectra in p+Be (left window) and p+Au (right window) collisions at 450 GeV.

3. DILEPTON PRODUCTION

The main contributions to dileptons with mass below 1.2 GeV are the Dalitz decay of π^0 , η and ω , the direct leptonic decay of ρ^0 , ω and ϕ , the pion-pion annihilation which proceeds through the ρ^0 meson, and the kaon-antikaon annihilation that proceeds through the ϕ meson. The differential widths for the Dalitz decay of π^0 , η , and ω are related to their radiative decay widths via the vector dominance model, which are taken from Ref. [25].

The decay of a vector meson into the dilepton is determined by the width,

$$\Gamma_{V \rightarrow l+l-}(M) = C_{l+l-} \frac{m_V^4}{3M^3} \left(1 - \frac{4m_l^2}{M^2}\right)^{1/2} \left(1 + \frac{2m_l^2}{M^2}\right). \quad (2)$$

The coefficient C_{l+l-} in the dielectron channel is 8.814×10^{-6} , 0.767×10^{-6} , and 1.344×10^{-6} for ρ , ω , and ϕ , respectively, and is determined from the measured width. For the dimuon channel, these values are slightly larger.

In our model, dileptons are emitted continuously during the time evolution of the colliding system. The way the dilepton yield is calculated can be illustrated by the decay of a rho meson. Denoting, at time t , the differential multiplicity of neutral rho mesons by $dN_{\rho^0}(t)/dM$, then the differential dilepton production probability is given by

$$\frac{dN_{l+l^-}}{dM} = \int_0^{t_f} \frac{dN_{\rho^0}(t)}{dM} \Gamma_{\rho^0 \rightarrow l+l^-}(M) dt + \frac{dN_{\rho^0}(t_f)}{dM} \frac{\Gamma_{\rho^0 \rightarrow l+l^-}(M)}{\Gamma_{\rho}(M)}, \quad (3)$$

where t_f is the freeze-out time, which is found to be about 20 fm/c. The first term corresponds to dilepton emission before freeze out while the second term is from the decay of rho mesons still present at freeze out.

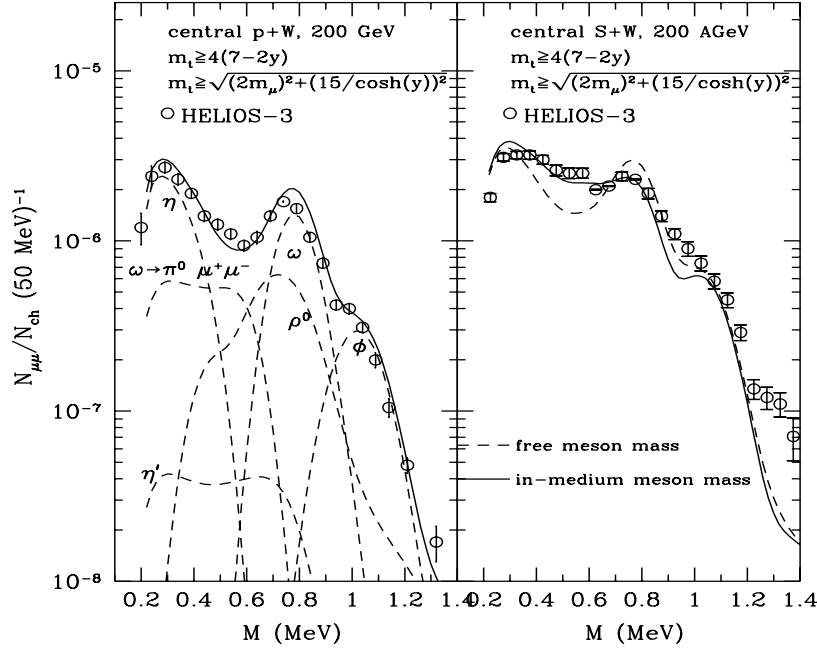


Figure 2. Dilepton invariant mass spectra in p+W (left window) and S+W (right window) collisions at 200 AGeV. In the right window the solid and dashed curves are obtained with in-medium and free meson masses, respectively.

The results for dilepton spectra from p+Be and p+Au collisions at 450 GeV are shown in Fig. 1, together with data from the CERES [1]. It is seen that the data can be well reproduced by Dalitz decay of π^0 , η and ω mesons, and direct leptonic decay of ρ^0 , ω and ϕ mesons. These results are thus similar to those found in Ref. [4] using the Hadron-String Dynamics and those constructed by the CERES collaboration from known and expected

sources of dileptons [1]. Similar conclusions can be drawn concerning dimuon spectra in p+W collisions at 200 GeV, which are shown in the left window of Fig. 2.

Our results for dilepton spectra in central S+Au collisions are shown in the left window of Fig. 3. The dashed curve is obtained with free meson masses. Although pion-pion annihilation is important for dileptons with invariant mass from 0.3 to 0.65 GeV, it still does not give enough number of dileptons in this mass region. Furthermore, for masses around $m_{\rho,\omega}$ there are more dileptons predicted by the theoretical calculations than shown in the experimental data. These are very similar to the results of Cassing *et al.* [4] based on the Hadron-String Dynamics model and Srivastava *et al.* [5] based on the hydrodynamical model. The results obtained with in-medium meson masses are shown by the solid curve. Compared with the results obtained with free meson masses, there is about a factor of 2-3 enhancement of the dilepton yield in the mass region from 0.2 to 0.6 GeV, which thus leads to a good agreement between the theoretical results and the CERES data. Similar conclusions that dropping vector meson masses can explain the CERES dilepton data have been obtained in Refs. [4,9,11].

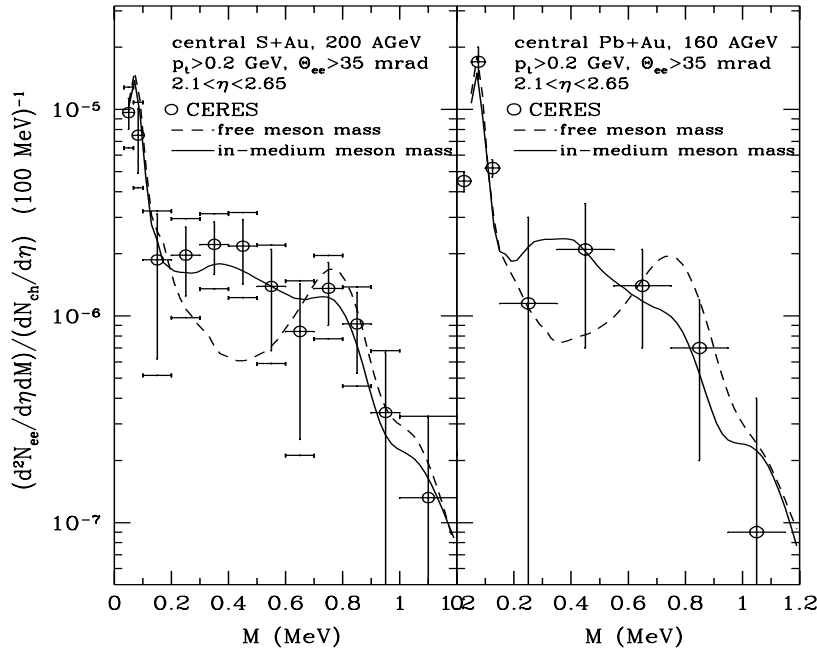


Figure 3. Dilepton invariant mass spectra in S+Au collision at 200 AGeV (left window) and Pb+Au collisions at 160 AGeV (right window). The solid and dashed curves are obtained with in-medium and free meson masses, respectively.

In the right window of Fig. 3 we compare our prediction for central Au+Pb collisions at

160 AGeV with the preliminary data from the CERES collaboration. The normalization factor $dN_{ch}/d\eta$ here is the average charge particle pseudo-rapidity density in the pseudo-rapidity range of 2 to 3, and is about 440 in this collision. In the results with free meson masses, shown by the dashed curve, there is a strong peak around $m_{\rho,\omega}$, which is dominated by ρ^0 meson decay as a result of an enhanced contribution from pion-pion annihilation in Pb+Au collisions than in S+Au and proton-nucleus collisions. In the case of in-medium meson masses, shown by the solid curve, the ρ meson peak shifts to a lower mass, and the peak around $m_{\rho,\omega}$ becomes a shoulder arising mainly from ω meson decay. At the same time we see an enhancement of low-mass dileptons in the region of 0.25-0.6 GeV as in S+Au collisions. The agreement with the data is thus significantly improved when dropping vector meson masses are used.

The same model has been used to calculate the dimuon spectra from central S+W collisions. The results obtained with free meson masses are shown in the right window of Fig. 2 by the dashed curve, and are below the HELIOS-3 data in the mass region from 0.35 to 0.6 GeV, and slightly above the data around $m_{\rho,\omega}$ as in the CERES case. However, the discrepancy between the theory and the data is somewhat smaller in this case due to the smaller charged-particle multiplicity at a larger rapidity than in the CERES experiment. Our results obtained with in-medium meson masses are shown in the right window of Fig. 2 by the solid curve, and are in good agreement with the data. The importance of dropping rho meson mass in explaining the HELIOS-3 data has also been found by Cassing *et al.* [4].

4. PHOTON PRODUCTION

Single photon spectra in heavy-ion collisions at CERN-SPS energies have been measured by the WA80 collaboration [16]. So far, only the upper bound has been determined for the so-called ‘thermal’ photon spectra, which accounts for about 5% of the total observed single photon yield, which is dominated by neutral pion decay. In hydrodynamical calculations [17], the absence of significant thermal photons has been interpreted as an evidence for the formation of a quark gluon plasma. Without phase transition, the initial temperature of the hadronic gas found in Ref. [17] is about 400 MeV. This leads to a large number of thermal photons from hadronic interaction which is not observed experimentally. Including the phase transition, the initial temperature is lowered to about 200 MeV [17], because of increased degrees of freedom. With a lower initial temperature, the thermal photon yield is thus reduced and is found to better agree with the WA80 data. However, a more recent analysis [26] has shown that if one includes all hadron resonances with masses below 2.5 GeV the initial temperature can also be lowered to about 200 MeV, and the WA80 photon data can then be explained without invoking the formation of a quark gluon plasma. This is basically also the conclusion of the detailed transport model analysis presented here.

For the ‘thermal’ photon spectra we include the decay of ρ , ω , η' , and a_1 mesons, as well as two-body processes such as $\pi\pi \rightarrow \rho\gamma$ and $\pi\rho \rightarrow \pi\gamma$. The decay width for $\rho \rightarrow \pi\pi\gamma$ is taken from the model of Ref. [27], which describes well the measured width for $\rho^0 \rightarrow \pi\pi\gamma$. Both the ω and a_1 radiative decay widths are proportional to $|\mathbf{p}_\pi|^3$ [28], with the coefficients determined from the measured width. For the two-body cross sections,

we use the results of [29], which do not include the contribution from an intermediate a_1 meson. The latter has already been included in our model as a two-step process.

In Fig. 4, our results for ‘thermal’ photon spectra are compared with the upper bound from the WA80 collaboration. It is seen that the ω meson radiative decay plays an important role for photons with transverse momenta above 300 MeV. In both the free and in-medium meson mass scenarios, our thermal photon yields do not exceed the experimental upper bound. Although there are more rho and a_1 mesons in the case of in-medium meson masses, their contributions to single photon yield do not increase significantly, simply because their radiative decay widths decrease as a result of reduced phase space.

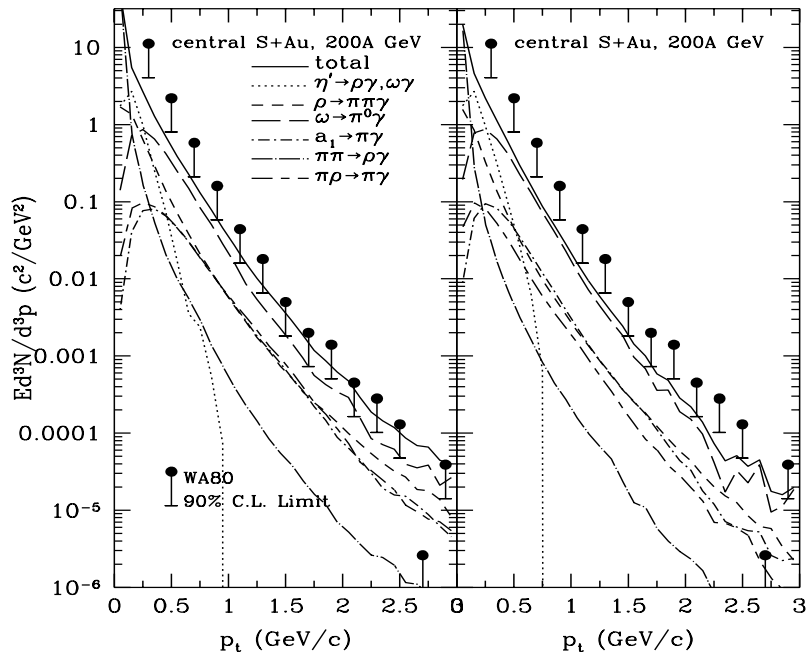


Figure 4. ‘Thermal’ photon spectra in central S+Au collisions at 200 AGeV using free (left window) and in-medium (right window) meson masses.

5. SUMMARY AND OUTLOOK

In summary, we have studied dilepton production from both proton-nucleus and nucleus-nucleus collisions using the relativistic transport model with initial conditions determined by string fragmentation from the initial stage of the RQMD model. It is found that the dilepton spectra in proton-nucleus reactions measured by the CERES and the HELIOS-3 collaboration can be well understood in terms of conventional mechanisms of Dalitz decay

and direct vector meson decay. For dilepton spectra in central heavy-ion collisions, these conventional mechanisms, however, fail to explain the data, especially in the low-mass region from about 0.25 to about 0.6 GeV in CERES experiments, and from 0.35 to 0.65 GeV in HELIOS-3 experiments. Including the contribution from pion-pion annihilation, which is important in the mass region from $2m_\pi$ to $m_{\rho,\omega}$, removes some of the discrepancy. But the theoretical prediction is still substantially below the data in the low mass region and somewhat above the data around $m_{\rho,\omega}$. The theoretical results are brought into good agreement with the data when reduced in-medium vector meson masses are taken into account. We have also calculated, within the same dynamical model, the thermal photon spectra in central S+Au collisions. In both free meson masses and in-medium meson masses scenarios, our results do not exceed the upper bound deduced from the experiments by the WA80 collaboration.

REFERENCES

1. G. Agakichiev *et al.*, Phys. Rev. Lett. 75 (1995) 1272; J. P. Wurm for the CERES Collaboration, Nucl. Phys. A590, 103c (1995); I. Tserruya, Nucl. Phys. A590 (1995) 127c; A. Drees, Nucl. Phys. A610 (1996) 536c.
2. M. Masera for the HELIOS-3 Collaboration, Nucl. Phys. A590 (1995) 93c.
3. G. Q. Li, C. M. Ko, and G. E. Brown, Phys. Rev. Lett. 75 (1995) 4007; Nucl. Phys. A606 (1996) 568; G. Q. Li, C. M. Ko, G. E. Brown, and H. Sorge, *ibid.* A611 (1996) 539; A610 (1996) 342c.
4. W. Cassing, W. Ehehalt, and C. M. Ko, Phys. Lett. B363 (1995) 35; W. Cassing, W. Ehehalt, and I. Kralik, *ibid.* B377 (1996) 5.
5. D. K. Srivastava, B. Sinha, and C. Gale, Phys. Rev. C53 (1996) R567.
6. R. Rapp, G. Chanfray, and J. Wambach, Phys. Rev. Lett. 76 (1996) 368; B. Friman, Nucl. Phys. A610 (1996) 358c; F. Klingl and W. Weise, Nucl. Phys. A606 (1996) 329.
7. V. Koch and C. S. Song, Phys. Rev. C 54 (1996) 1903.
8. J.V. Steele, H. Yamagishi, and I. Zahed, Phys. Lett. B 384 (1996) 255.
9. C. M. Hung and E. Shuryak, hep-ph/9608299.
10. J. Sollfrank, P. Huovinen, M. Kataja, P.V. Ruuskanen, M. Prakash, and R. Venugopalan, Phys. Rev. C55 (1997) 392.
11. R. Baier, M. Dirks, and K. Redlich, Phys. Rev. D55 (1997) 4344.
12. J. Murray, W. Bauer, and K. Haglin, hep-ph/9611328.
13. G.E. Brown and M. Rho, Phys. Rev. Lett. 66 (1991) 2720.
14. J. Kapusta, D. Kharzeev, and L. McLerran, Phys. Rev. D 53 (1996) 5028; Z. Huang and X.-N. Wang, *ibid.* 5041.
15. A. Drees, Phys. Lett. B 338 (1996) 380
16. R. Albrecht *et al.*, Phys. Rev. Lett. 76 (1996) 3506.
17. D. K. Srivastava and B. Sinha, Phys. Rev. Lett. 73 (1994) 2421; A. Dumitru *et al.*, Phys. Rev. C 51 (1995) 2166.
18. C. M. Ko, Q. Li, and R. Wang, Phys. Rev. Lett. 59 (1987) 1084; C. M. Ko and Q. Li, Phys. Rev. C37 (1988) 2270.
19. B. D. Serot and J. D. Walecka, Adv. Nucl. Phys. 16 (1986) 1.
20. H. Sorge, H. Stöcker, and W. Greiner, Ann. Phys. 192 (1989) 266.

21. T. Hatsuda and S. H. Lee, Phys. Rev. C46 (1992) R34.
22. K. Saito and A. W. Thomas, Phys. Rev. C51 (1995) 2757.
23. R.J. Furnstahl, H.-B. Tang, and B.D. Serot, Phys. Rev. C 52 (1995) 1368.
24. G.Q. Li, G.E. Brown, C.-H. Lee, and C.M. Ko, to be published.
25. L. G. Landberg, Phys. Rep. 128 (1985) 301.
26. J. Cleymans, K. Redlich, and D.K. Srivastava, Phys. Rev. C 55 (1997) 1431.
27. P. Singer, Phys. Rev. 130 (1963) 2441.
28. Ö. Kaymakçalan, S. Rajeev, and J. Schechter, Phys. Rev. D 30 (1984) 594; L. Xiong, E. Shuryak, and G.E. Brown, Phys. Rev. D 46 (1992) 3798.
29. J. Kapusta, P. Lichard, and D. Seibert, Phys. Rev. D 44 (1991) 2774.